Mesoporous Ru/MgO prepared by a deposition-precipitation method as highly active catalyst for producing CO_x-free hydrogen from ammonia decomposition

Xiaohua Ju [a], Lin Liu [a,*], Pei Yu [a], Jianping Guo [a], Xilun Zhang [a,b], Teng He [a], Guotao Wu [a], Ping Chen [a,*]

[a] Dalian National Laboratory for Clean Energy, State Key Laboratory of Catalysis, Dalian Institute of Chemical Physics, Chinese Academy of Sciences, Dalian 116023, PR China
[b] University of Chinese Academy of Sciences, Beijing 100049, PR China

ARTICLE INFO

ABSTRACT

Development of highly active catalyst for producing CO_x-free H_2 from ammonia decomposition is critical for the utilization of ammonia as H_2 carrier in proton exchange membrane fuel cell. Here, we present a deposition–precipitation (DP) method towards the synthesis of a highly active and stable mesoporous Ru/MgO catalyst for NH_3 decomposition reaction. Nitrogen sorption measurements show that the deposition–precipitation method can introduce mesoporosity into the Ru/MgO-DP catalysts. Much enhanced Ru dispersion can be observed for the mesoporous Ru/MgO-DP catalysts in comparison with that of the Ru/MgO catalysts prepared by impregnation method due to the high surface area and plenty of mesopores of the Ru/MgO-DP catalysts. As a result, the mesoporous Ru/MgO-DP catalysts show significantly improved catalytic activity for NH_3 decomposition. The activity of Ru/MgO-DP catalyst can be further remarkable enhanced with KOH, which can give comparable catalytic performance with that of the most efficient carbon nanotube supported Ru catalyst.

© 2017 Elsevier B.V. All rights reserved.

1. Introduction

Hydrogen has been recognized as one of the most promising energy carriers for future energy systems. Up to now, the storage of hydrogen is still one of the obstacles for the promising applications. Recent years, ammonia has attracted increasing attention as a medium for storage of hydrogen [1,2]. Ammonia has many advantages such as high gravimetric (17.7 wt% H_2) and volumetric H_2 density, high energy density, liquid state under mild conditions (20 °C and 0.8 MPa) and billion tons of annual production. Thus, NH_3 may play a promising role as H_2 carrier in implementation of a future hydrogen economy [3,4]. Currently, generation of CO_x-free H_2 via NH_3 decomposition has attracted considerable attention in terms of energy storage and economic benefit with the rapid progresses in the research and development of proton-exchange membrane fuel cells (PEMFC) [5–16].

Release of CO_x-free H_2 from NH_3 as hydrogen source for PEMFC relies on the availability of highly active catalysts for NH_3 decom-

position, especially at relative low temperatures. During the past years, a variety of effective catalyst systems such as metals, metal carbides [17], and metal nitrides [17–22] have been developed for NH_3 decomposition. Metal catalysts, such as Ru [11,14,23–25], Ir [11,24], Rh [14,24], Pt [14], Pd [14,24], Fe [14,24,26], Co [24,27] and Ni [11,12,14,28,29], exhibited high activities for NH_3 decomposition, and among which Ru was found to be the most active metal catalyst [11,14,23,24]. Yin et al. showed that Ru supported on carbon nanotubes (CNTs) was highly active for NH_3 decomposition [13,14,23]. However, methanation reaction of the CNTs support in H_2 atmosphere is adverse for the stability of Ru/CNTs catalyst. Hayashi et al. found that Ru-loaded inorganic electride (C12A7:e-) exhibited high activity for NH_3 decomposition [30]. However, the relatively low stability of electrides under ambient conditions will restrict the practical application of Ru/C12A7:e-.

Experimental observations have revealed that the catalytic activity of Ru-based catalysts in NH_3 decomposition is support-dependent, that is, the catalytic activities of Ru-based catalysts in NH_3 decomposition vary greatly with the properties of the support. Among Ru-based catalysts supported on a variety of supports, such as SiO_2 [31,32], TiO_2 [14], zeolite [32], Al_2O_3 [33,34], MgO [14,35], activated carbon [14,36], carbon nanotubes [13–15,20,23,25,37]

and C12A7 electrides [30], Ru/MgO catalyst has received special attention due to its high catalytic activity and stability. However, the catalytic activities of Ru/MgO catalysts are still need to be further improved. Up to now, most of the Ru/MgO catalysts for NH_3 decomposition were prepared by the impregnation method, and the activities of Ru/MgO catalysts at low temperature need to be further improved. During the past years, several approaches have been taken to synthesize highly active Ru/MgO catalysts in NH_3 decomposition. Xu and co-workers reported the preparation of a highly active Ru/MgO catalyst through a polyol reduction method [38]. The highly dispersed Ru nanoparticles supported on MgO possessed relatively high activity in NH_3 decomposition.

To enhance the catalytic performances of Ru/MgO catalysts, Ru/MgO catalysts with plenty of accessible mesopores and large surface areas are especially attractive due to the plenty of active sites on the surface. The mesoporous Ru/MgO catalysts can not only facilitate the mass transfer in catalytic reactions, but also promote the dispersion of Ru metal particles. In this work, mesoporous Ru/MgO catalyst with high surface area has been prepared by a urea-based deposition–precipitation method, and investigated for NH_3 decomposition. The mesoporous Ru/MgO-DP catalyst showed much improved activity in comparison with that of the conventional Ru/MgO catalyst prepared by impregnation method. The physicochemical properties of mesoporous Ru/MgO-DP catalysts were characterized by different structure characterization techniques. The exceptional catalytic performances of mesoprous Ru/MgO-DP catalysts can be mainly ascribed to the high surface areas of the catalysts and high dispersions of Ru nanoparticles on the surface of MgO supports. Additionally, the catalytic activity of Ru/MgO-DP catalysts can be significantly promoted with a small amount of KOH.

2. Experimental

2.1. Catalyst preparation

The Ru/MgO catalysts with Ru loading of 3.0 wt.% and 5.0 wt.% were prepared by DP method, which has been widely used for the synthesis of transition-metal oxide-supported gold catalysts [39,40]. The analytic grade $RuCl_3 \cdot xH_2O$ precursor was purchased from Tianjin jinbolan company. $RuCl_3 \cdot xH_2O$ ($n(RuCl_3):n(HNO_3) = 1:10$) (0.60 mL, 55.76 g/L) aqueous solution was first mixed with 0.30 g of MgO powder (Shenyang chemical reagent plant, China) and then diluted with 30 mL of deionized water. This suspension was vigorously stirred for 1 h at ambient temperature. Subsequently, a designated amount of urea with a molar ratio of Ru to urea at 1:200 was added as the precipitation agent. The mixture was reacted at 80 °C for 8 h and aged at room temperature for 12 h. The product was obtained by filtration to separate the precipitate from the solution, and then washed for three times with deionized water. Finally, the product was dried at 80 °C for 6 h. The catalysts were identified as x%Ru/MgO-DP, where x corresponding to the weight percent of Ru metal in the catalysts. Before the catalytic test, the sample was reduced in flowing NH_3 at 500 °C for 2 h to obtain the reduced catalysts.

The KOH modified Ru/MgO-DP catalysts were prepared by wet impregnation of reduced Ru/MgO-DP catalyst with KOH solution in ethanol, followed by drying at 80 °C overnight and calcination at 500 °C for 2 h in Ar flow.

To understand the influence of DP method on the catalytic performance of Ru/MgO-DP catalyst, Ru/MgO samples prepared by incipient wetness impregnation and were used as reference samples for comparison with Ru/MgO-DP catalysts. The concentration of $RuCl_3 \cdot xH_2O$ was 25 mg/mL. The acetone solution was added to the MgO support and stirred for 20 min, and then the solvent was

removed in air to obtain the air-dry sample. Subsequently, the sample was dried at 80 °C for another 2 h. After that, the sample was heated in flowing Ar to 550 °C for 2 h. The obtained catalysts were denoted as x%/Ru/MgO-IM, where x corresponding to the weight percent of Ru metal in the catalysts. Before the catalytic test, the samples were reduced in flowing NH_3 at 500 °C for 2 h to obtain the reduced catalysts.

2.2. Catalyst characterization

The Ru metal content in $RuCl_3 \cdot xH_2O$ was determined by inductively coupled plasma-atomic emission spectroscopy (ICP-AES, Optima 2000DV, USA). The x value determined from ICP is 5.4, and which was used for determine the metal loading in Ru/MgO catalysts. Powder X-ray diffraction (XRD) patterns were recorded on an X'Pert Pro (PANAlytical) diffractometer with Cu Ka radiation at 40 kV and 40 mA. Nitrogen adsorption/desorption isotherms were measured with a Micromeritics ASAP 2020 analyzer at −196 °C. The samples were degassed in a vacuum at 300 °C for 8 h before the measurements. The surface areas were determined by applying the Brunauer-Emmett-Teller (BET) method. The pore diameter and distribution were obtained by using the Barrett-Joyner-Halenda (BJH) method.

Temperature-programmed reduction (TPR) was operated in a home-made apparatus. Prior to each measurement, the sample (0.1 g) was heated from room temperature to 350 °C with a heating rate of 10 °C/min under Ar flow (30 mL/min), and kept at 350 °C for 30 min to remove the adsorbed impurities (e.g. H_2O). After being cooled to room temperature, the gas flow was switched to 5% H_2/Ar (30 mL/min) and reduced the sample with a temperature ramp of 10 °C/min. The TPR profiles were measured with a gas chromatograph equipped with thermal conductivity (TCD) detector.

The exposed Ru surface area was measured by CO pulse chemisorption using an automated chemisorption analysis instrument from Altamira (AMI-200). The catalyst was loaded into a 1/4 inch quartz tube for each test. Prior to the pulse CO chemisorption measurement, the catalyst was reduced at 450 °C for 2 h in 10% H_2 (balance with Ar), and then cooled down to room temperature in He. CO pulses were introduced to the sample (250 mL of pure CO) and the CO uptake was measured using a gas chromatography equipped with TCD detector. The Ru dispersion was calculated by assuming a CO:Ru stoichiometry of 1:1.

The morphology characterization was performed on a JEOL 2100X transmission electron microscope operating at 200 kV. The catalyst powders were dispersed in ethanol by ultrasonic and then a drop of the solution was placed on a carbon-coated copper grid.

XAFS measurements: XAFS experiments were performed at the BL14W beamline of Shanghai Synchrotron Radiation Facility. Samples were pressed into pellets and then sealed with KAPTON film on both sides to avoid air contamination. Ru K-edge spectra of Ru/MgO-DP and Ru/MgO-IM samples were measured at room temperature using a Si(311) double-crystal monochromator in transmission model. The X-ray energy was calibrated using a standard Ru foil. Data Analysis of the XAFS spectra was conducted with Athena and Artemis in the LFEFFIT package. The k3-weighted EXAFS oscillation in the range 2–13 Å was Fourier-transformed into R-space after background subtraction.

2.3. Catalyst evaluation

Catalytic testing was carried out on a continuous fixed-bed flow quartz reactor (catalyst: 50 mg, 40–60 mesh) under pure NH_3 with a flow rate of 30 mL min^{-1}. Prior to the reaction, the dried catalysts were heated in an Ar flow (30 mL/min) from room temperature to 300 °C with a heating rate of 5 °C/min. The gas was switched to NH_3 (30 mL/min) when the temperature reached 300 °C and
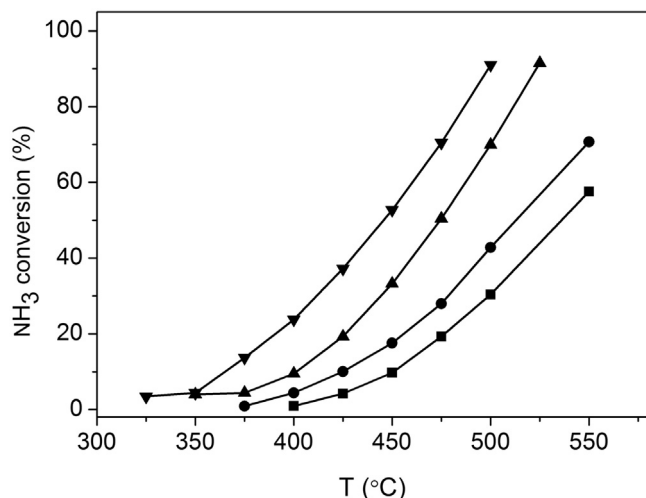
Fig. 1. NH$_3$ conversion as a function of reaction temperature over Ru/MgO catalysts prepared from different methods: (■) 3%Ru/MgO-IM; (●) 5%Ru/MgO-IM; (▲) 3%Ru/MgO-DP; (▼) 5%Ru/MgO-DP.

Fig. 2. Effect of GHSV on catalytic performance of 5%Ru/MgO-DP catalyst for NH$_3$ decomposition: (■) 500 °C; (●) 475 °C; (▲) 450 °C.

Fig. 3. Stability test of the 5%Ru/MgO-DP catalyst for NH$_3$ decomposition. Reaction condition: 500 °C, GHSV = 36,000 mL/gcat·h.

the samples were continuously heated up to 500 °C with a heating rate of 5 °C/min. The Ru/MgO catalysts could be obtained after reduction in a NH$_3$ flow at 500 °C for 2 h. All the activity tests of the reduced Ru/MgO catalysts were conducted in the temperature range of 300–550 °C under the atmospheric pressure with a gas hourly space velocity (GHSV) of 36,000 mL/gcat·h. The gas composition was analyzed using on-line gas chromatography (GC-2014C, Shimadzu) equipped with a TCD detector and Poropak Q column, using H$_2$ as carrier gas.

3. Results and discussion

3.1. Catalytic activities of Ru/MgO catalysts prepared from different method

The catalytic performances of Ru/MgO catalysts prepared by different methods were investigated under identical reaction condition. Fig. 1 shows the NH$_3$ conversion as a function of temperature over the Ru/MgO catalysts prepared by different methods with a GHSV of 36,000 mL/gcat h. It can be seen that the NH$_3$ conversion increases with the reaction temperature for all the Ru/MgO samples, which is in agreement with the mild endothermic reaction of NH$_3$ catalytic decomposition. The activities of Ru/MgO catalysts for NH$_3$ decomposition follow the order of 5%Ru/MgO-DP > 3%Ru/MgO-DP > 5%Ru/MgO-IM > 3%Ru/MgO-IM, and the 5%Ru/MgO-DP sample gives the highest activity among the different samples. The activity of 5%Ru/MgO-IM catalyst is relatively low, and 5%Ru/MgO-IM only gives a NH$_3$ conversion about 17.5% at 450 °C. The catalytic activity of 5%Ru/MgO-DP shows a remarkable enhancement in comparison with that of the 5%Ru/MgO-IM catalyst. A comparison of our 5%Ru/MgO-DP catalyst with the Ru catalysts in the literature is listed in Table 1. The NH$_3$ conversion of 5%Ru/MgO-DP is about 52.7% at 450 °C, which is superior to most of the supported Ru catalysts reported in literatures (Table 1). The calculation of H$_2$ formation rate of catalyst per gram was based on the weight of the reduced 5%Ru/MgO-DP catalyst regardless of Ru content of the 5%Ru/MgO-DP catalyst. It can also be found that the obtained 5%Ru/MgO-DP catalyst possessed a much higher H$_2$ formation rate than the most efficient Ru/CNTs and Ru/MgO similar reaction condition. At 500 °C, 5%Ru/MgO-DP gives NH$_3$ conversion of 91.0%, which are much higher than that of the 5%Ru/MgO-IM (42.8%). Remarkably, the catalytic activity of 3%Ru/MgO-DP is higher than that of
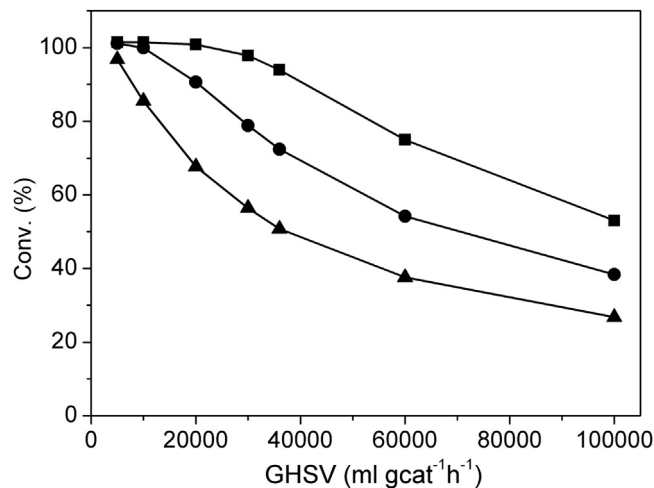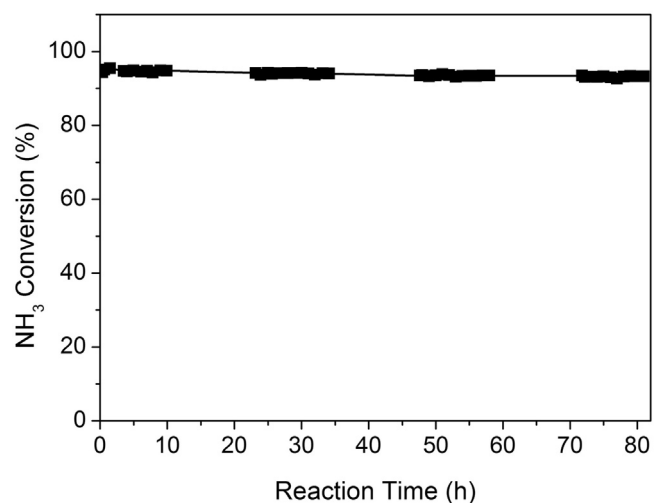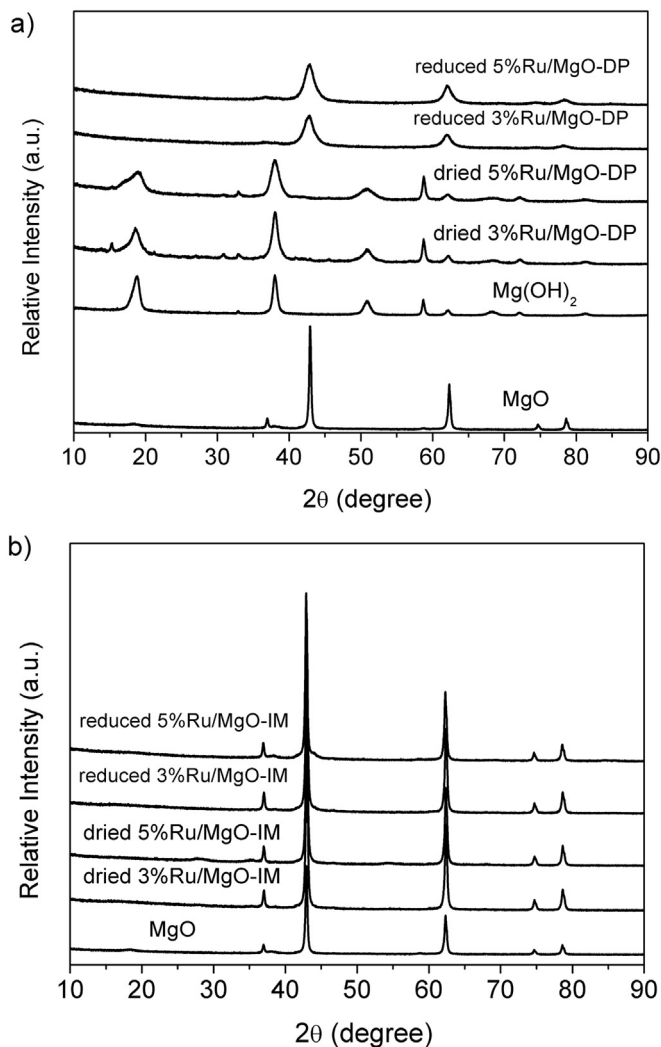
the 5%Ru/MgO-IM sample, even the 5%Ru/MgO-IM sample has an improved Ru content. Fig. 2 depicts the effect of GHSV on the catalytic performance of 5%Ru/MgO-DP catalyst. It can be seen that NH$_3$ conversion decreases with the increase of GHSV, indicating that relatively low GHSV is beneficial for NH$_3$ decomposition. Even though, above 90.0% NH$_3$ conversion can be obtained at 500 °C with a high GHSV of 36,000 mL/gcat h.

Additionally, the stability is useful for evaluating the catalytic performance of 5%Ru/MgO-DP catalyst. For carbon supported Ru catalyst, it is still challenging to maintain long-term durability for NH$_3$ decomposition due to the inevitable methanation of carbon material in a hydrogen condition at high reaction temperature. At a space velocity of 36,000 mL/gcat h, the stability of 5%Ru/MgO-DP catalyst was also investigated at 500 °C. As shown in Fig. 3, the catalytic activity remains almost unchanged during the 80 h test period, evidencing the high stability of the 5%Ru/MgO-DP catalyst in NH$_3$ decomposition reaction. Such a feature of the 5%Ru/MgO-DP catalyst demonstrated clearly that 5%Ru/MgO-DP catalyst is stable for NH$_3$ decomposition, which is important for a potential industrial application in a large scale.

Table 1

NH_3 conversion over un-promoted Ru catalysts at 450 °C and atmospheric pressure (GHSV: 30,000 mL/gcat h).

Catalyst	Preparation method	Ru weight loading (%)	NH_3 conversion (%)	H_2 formation rate (mmol/gcat min)	Reference
Ru/Al_2O_3	Impregnation[a]	10	31.5	11.5	[8]
Ru/SiO_2	Impregnation[a]	10	34.5	11.4	[8]
Ru/CNTs	Impregnation[b]	4.8	43.3	14.5	[16]
Ru/MgO	Impregnation[b]	4.8	30.8	10.3	[16]
Ru/TiO_2	Impregnation[b]	4.8	27.2	9.1	[16]
Ru/Al_2O_3	Impregnation[b]	4.8	23.3	7.8	[16]
Ru/AC	Impregnation[b]	4.8	28.7	9.6	[16]
Ru/MgO	Polyol reduction	2.8	41.3	13.8	[41]
5%Ru/MgO-DP	deposition–precipitation	3.5	56.5	18.9	This work

[a] Prepared by wetness incipient impregnation with water as solvent.

[b] Prepared by wetness incipient impregnation with acetone as solvent.

Fig. 4. (a) XRD patterns of MgO support, Mg(OH)$_2$, dried 3%Ru/MgO-DP, dried 5%Ru/MgO-DP, reduced 3%Ru/MgO-DP and reduced 5%Ru/MgO-DP. (b) XRD patterns of MgO support, dried 3%Ru/MgO-IM, dried 5%Ru/MgO-IM, reduced 3%Ru/MgO-IM and reduced 5%Ru/MgO-IM.

3.2. Characterizations

3.2.1. XRD

In order to reveal why the catalytic activities of Ru/MgO-DP samples are much higher than that of Ru/MgO-IM samples with similar composition, XRD was applied to characterize the structure of Ru/MgO-DP and Ru/MgO-IM samples. Fig. 4 shows XRD patterns of the dried and reduced Ru/MgO samples prepared from

different methods. For a comparison, the XRD patterns of MgO support and Mg(OH)$_2$ were also included. For dried Ru/MgO-DP samples (Fig. 4a), the diffraction peaks corresponding to the Mg(OH)$_2$ appeared in the dried Ru/MgO-DP samples along with the disappearance of peaks assigned to MgO phase, indicating the transformation of MgO support into Mg(OH)$_2$ occurred during the preparation process (Fig. 4a). After reduction in pure NH$_3$ at 500 °C, only characteristic peaks of MgO can be observed in the XRD patterns of the reduced Ru/MgO-DP samples as a result of thermal decomposition of Mg(OH)$_2$. It should be noted that no diffraction features attributable to Ru metal particles could be identified in the XRD patterns of the reduced Ru/MgO-DP samples, suggesting the crystal size of the Ru particles was too small to be detected. Different from the Ru/MgO-DP samples, only diffraction peaks corresponding to the MgO support can be observed in the XRD patterns of the dried and reduced Ru/MgO-IM samples (Fig. 4b). For the reduced Ru/MgO-IM samples, besides the diffraction lines of MgO support, a very small broad peak at 44.02° corresponding to Ru metal can also be observed.

3.2.2. N$_2$ sorption

Fig. 5 shows the N$_2$ adsorption/desorption isotherms and pore size distributions of MgO support, reduced Ru/MgO-IM and reduced Ru/MgO-DP samples. As found in Fig. 5a, Ru/MgO-IM samples give similar nitrogen sorption isotherms with that of the MgO support. However, the nitrogen sorption isotherms of Ru/MgO-DP catalysts are remarkably different from that of the MgO support. The Ru/MgO-DP samples show a significant increase in adsorption capacity in relative to the MgO support. The Ru/MgO-DP catalysts exhibit type IV isotherms with an H3 hysteresis as defined by the IUPAC. The hysteresis loop observed in the relative pressure P/P$_0$ between 0.6 and 1.0 indicates the formation of distinct mesoporosity in the Ru/MgO-DP samples. Development of mesoporous structure in the Ru/MgO-DP samples can be further proved by the pore size distribution curves (Fig. 5b), and it can be seen that both the 3%Ru/MgO-DP and 5%Ru/MgO-DP show relatively narrow mesopore size distribution centered at about 2.9 nm. As HNO$_3$ was added together with the RuCl$_3$ precursor, part of the MgO support can react with HNO$_3$ and form soluble Mg(NO$_3$)$_2$. During the deposition–precipitation process, urea can release NH$_3$ at 90 °C slowly, and the soluble Mg(NO$_3$)$_2$ can slowly precipitated in the form of nanostructured Mg(OH)$_2$, which can be proved by XRD results shown in Fig. 4a. XRD results reveal that MgO support can be converted into Mg(OH)$_2$ during the deposition–precipitation process. In the following high temperature reduction treatment at 500 °C, the nanostructured Mg(OH)$_2$ can be converted back into the nanostructured MgO and disordered mesopores can be formed simultaneously as a result of structure transformation. As a result, the nanostructured MgO shows much broader diffraction peaks in comparison with that of the parent MgO due to the much lower crystallinity. The well-defined mesoporous structure of Ru/MgO-
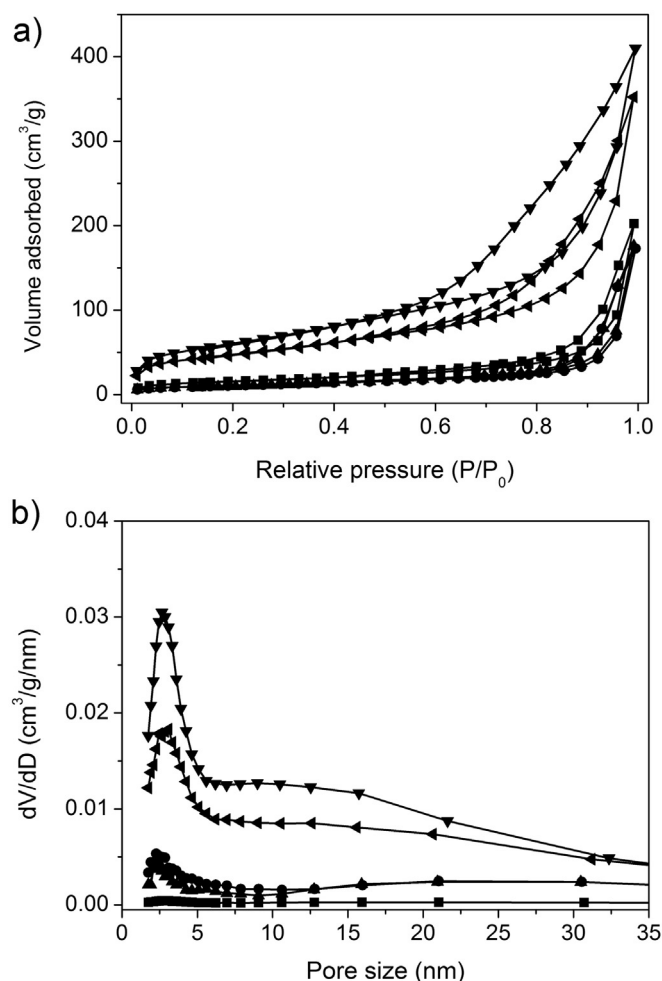
a)

b)

Fig. 5. N$_2$ sorption isotherms (a) and pore size distribution curves (b) of (■) MgO support, (●) reduced 3%Ru/MgO-IM, (▲) reduced 5%Ru/MgO-IM, (▼) reduced 3%Ru/MgO-DP and (◄) reduced 5%Ru/MgO-DP samples.

DP can not only provide more active sites, but also facilitate the mass transfer in NH$_3$ decomposition reaction. The textural properties of Ru/MgO samples derived from N$_2$ sorption experiments are summarized in Table 1. It can be seen that loading Ru species by impregnation method results in the decrease in the surface areas of Ru/MgO-IM samples. The surface areas of 3%Ru/MgO-IM and 5%Ru/MgO-IM are only 38.4 and 40.7 m^2/g respectively, which are smaller than that of the MgO support (56.2 m^2/g). Different from the Ru/MgO-IM samples, a remarkable increase in the surface areas can be observed for the Ru/MgO-DP samples. Compared with the MgO support, a 3.9-fold and 3.0-fold increase of surface areas can be observed for 3%Ru/MgO-DP and 5%Ru/MgO-DP samples, reaching 219.4 and 168.9 m^2/g, respectively. Compared with 3%Ru/MgO-DP sample, a little decrease in the surface area can be observed for 5%Ru/MgO-DP sample. The amount of HNO$_3$ in the reaction system can influence the dissolution and precipitation of Ru/MgO-DP during the preparation process, which may influence the structure of the nanostructured Mg(OH)$_2$ of the Ru/MgO-DP sample. Thus, 5%Ru/MgO-DP sample gives a relatively lower surface area in comparison with that of the 3%Ru/MgO-DP sample. The remarkable increase in the surface areas for Ru/MgO-DP catalysts correlates well with the much enhanced activity of Ru/MgO-DP in comparison with that of Ru/MgO-IM catalysts.
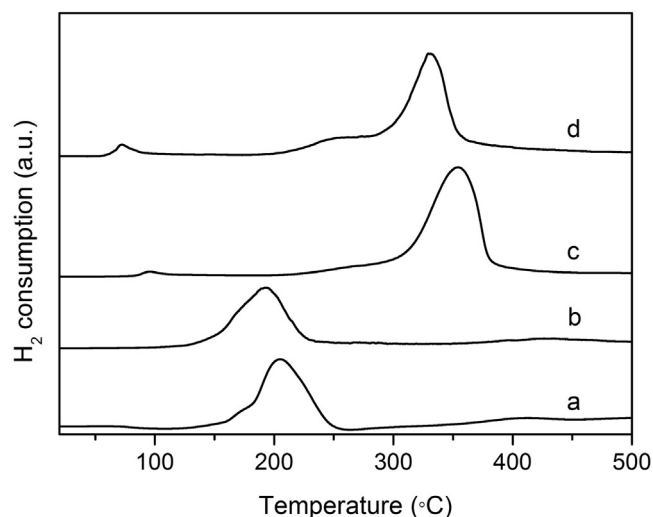

Fig. 6. TPR profiles of Ru/MgO catalysts: (a) 3%Ru/MgO-IM; (b) 5%Ru/MgO-IM; (c) 3%Ru/MgO-DP; (d) 5%Ru/MgO-DP.

3.2.3. H$_2$-TPR

The H$_2$-TPR technique has been often used to examine the strength of interaction between active component and support, and can provide useful information for catalyst activation and reduction. Here, H$_2$-TPR technique was applied to evaluate the interaction between Ru species and MgO support (Fig. 6). The reduction behavior of Ru/MgO sample is highly dependent on the preparation method. For the Ru/MgO-IM samples, the onset and peak reduction temperatures are about 130 and 200 °C, respectively. The onset and peak reduction temperatures of Ru species in mesoporous Ru/MgO-DP samples shift towards high temperature in comparison with that of the Ru/MgO-IM samples. The onset reduction temperatures for the 3%Ru/MgO-DP and 5%Ru/MgO-DP are 205 and 210 °C, which are much higher than that of the Ru/MgO-IM samples. For 3%Ru/MgO-DP and 5% Ru/MgO-DP, the peak reduction temperatures occur at about 350 and 330 °C. The shift of reduction temperature for the mesoporous Ru/MgO-DP catalyst could be directly attributed to the preparation method as the same composition of the mesoporous Ru/MgO-DP and Ru/MgO-IM samples. XRD results have shown that MgO can react with H$_2$O and converted into Mg(OH)$_2$. Along with the release of NH$_3$ from hydrolysis of urea during the preparation process, insoluble Ru species such as RuO$_x$(OH)$_y$, RuO$_2$·2H$_2$O, or Ru(OH)$_x$ can be precipitated from aqueous solution and deposited on surface of Mg(OH)$_2$ support. The newly precipitated Ru species on the surface of Mg(OH)$_2$ support result in a much enhanced interaction between Ru species and MgO supports than the conventional IM method, which may induce highly dispersion of Ru species on the surface of mesoporous Ru/MgO-DP samples.

3.2.4. EXAFS

Fig. 7 shows the k^3-weighted Fourier transform Ru K edge extended X-ray absorption fine structure (EXAFS) spectra of mesoporous Ru/MgO-DP and Ru/MgO-IM samples, together with Ru foil and RuO$_2$ reference samples. The EXAFS spectra (Fig. S1) and Fourier-transformed k-space spectra of the mesoporous Ru/MgO-DP and Ru/MgO-IM samples are similar and closely resemble that of Ru foil, but with a little reduced oscillations. All the mesoporous Ru/MgO-DP and Ru/MgO-IM catalysts exhibit strong peak at 2.33 Å due to Ru–Ru scattering, which are similar with that of the Ru foil. The presence of some Ru-O features in the 3%Ru/MgO-IM was evidenced by a shoulder at around 1.5 Å, which may be partially oxidized after the catalytic test due to the small particle size of the
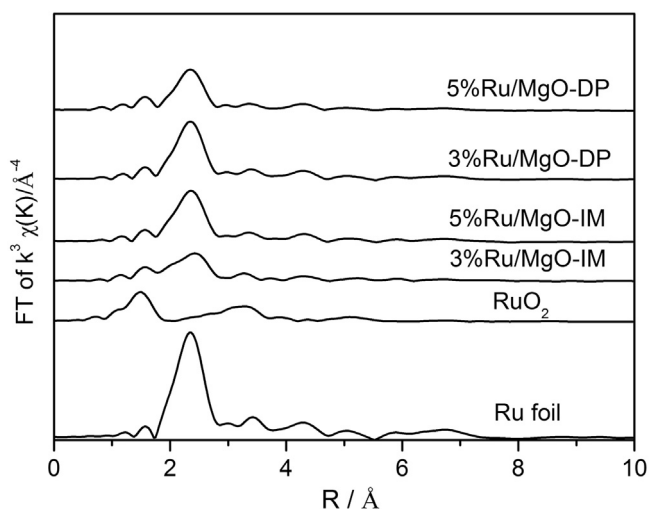
Fig. 7. The k^3-weighted Fourier transform Ru K-edge EXAFS spectra of Ru foil, RuO$_2$, 3%Ru/MgO-IM, 5%Ru/MgO-IM, 3%Ru/MgO-DP and 5%Ru/MgO-DP samples. The catalysts were measured after activity tests.

Ru nanoparticles. Compared with that of the Ru foil, the intensities of peak from the first shell Ru–Ru scattering show obvious decrease for mesoporous Ru/MgO-DP and Ru/MgO-IM samples. In addition, Ru K-edge X-ray absorption near edge structure (XANES) and k^3-weighted EXAFS spectra suggested the absence of RuO$_2$ in the reduced mesoporous Ru/MgO-DP and Ru/MgO-IM samples, which indicates that the Ru species in the catalysts have been completely reduced.

3.2.5. CO chemisorption

The Ru dispersion is a crucial factor for determining the catalytic performance of the Ru/MgO catalyst. From Table 2, it can be seen that the preparation method has a significantly influence on the dispersion degree of Ru metal on the MgO support. According to the CO chemisorption results (Table 2), the Ru dispersion values of 3%Ru/MgO-IM and 5%Ru/MgO-IM sample are only about 11.8% and 7.0%, respectively. The Ru dispersion values of 3%Ru/MgO-DP and 5%Ru/MgO-DP samples are 25.3% and 33.6% respectively, which are much higher than the corresponding Ru/MgO-IM samples with same Ru loading. It is apparent that the loading of Ru with DP method has a notable impact on the dispersion of Ru in mesoporous Ru/MgO-DP samples as a result of high surface area. The average Ru particle sizes of 3%Ru/MgO-DP and 5%Ru/MgO-DP catalysts evaluated by CO chemisorption were about 4.3 and 3.3 nm, which are much smaller than those of 3%Ru/MgO-IM and 5%Ru/MgO-IM samples. Consistent with the catalytic activity results, DP method induces a much enhanced dispersion of Ru on the surface of mesoporous Ru/MgO-DP catalysts. The turnover frequency (TOF) obtained over a catalyst has been used as a standard parameter for the measurement of catalytic performance. TOF$_{H2}$ could be calculated by normalizing the observed H$_2$ formation rate (mole formed, H$_2$/s/gcat) to the number of exposed Ru surface atoms per gram of catalyst. At 450 °C under the same condition, the TOF$_{H2}$ values of 3%Ru/MgO-DP and 5%Ru/MgO-DP catalysts are 4.0 and 3.0 s^{-1} respectively. Different from that of the Ru dispersion results, the 3%Ru/MgO-IM and 5%Ru/MgO-IM catalysts give relative higher TOF$_{H2}$ values than those of the corresponding Ru/MgO-DP catalysts. Unlike NH$_3$ conversion, the TOF over the Ru/MgO catalysts at 450 °C is ranked in the order of 5%Ru/MgO-IM > 3%Ru/MgO-DP > 5%Ru/MgO-DP > 3%Ru/MgO-IM. In NH$_3$ synthesis, Murata and Aika noted a rise in TOF over promoted Ru/Al$_2$O$_3$ catalysts with growth of size of Ru particles [41]. Liang et al. observed that TOF increased by a factor of 9 (from 0.004 to 0.036 s^{-1}) with the size of Ru particles changed from 1.7 to 10.3 nm over AC-supported Ru [42]. Similar to NH$_3$ synthesis reaction [41,42], the NH$_3$ decomposition reaction has also been proved to be structure sensitive [43]. Vlachos reported that NH$_3$ decomposition on Ru is highly structure sensitive, with TOF values increasing by almost 2 orders of magnitude as the particle size increases from 0.8 nm to >7 nm [43].
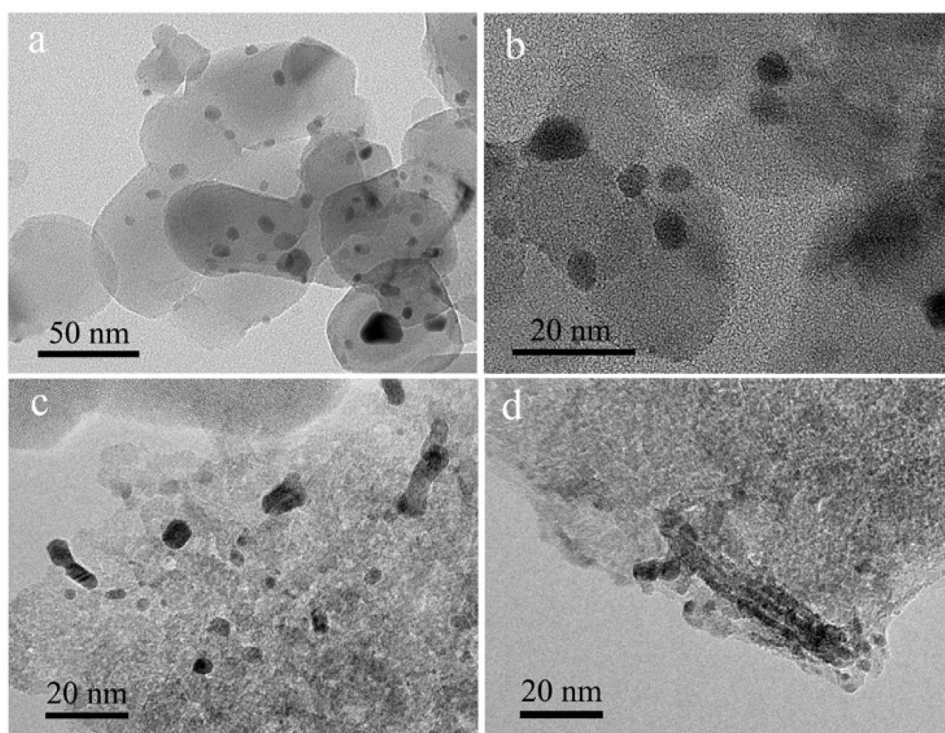

Fig. 8. TEM images of reduced (a) 3%Ru/MgO-IM, (b) 5%Ru/MgO-IM, (c) 3%Ru/MgO-DP and (d) 5%Ru/MgO-DP catalysts.

Table 2
Properties of the reduced Ru catalysts.

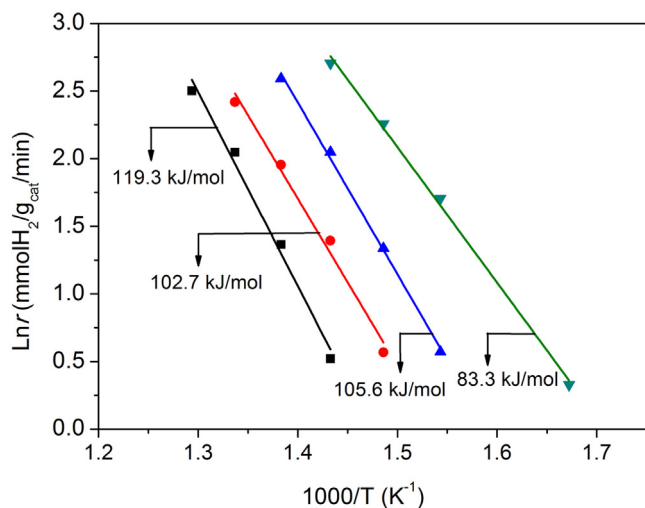| Catalysts	Metal loading (wt.%)	Surface area (m^2/g)	Metal dispersion by CO chemisorption (%)	Ru particle size by CO chemisorption (nm)	TOF_{H2} (s^{-1}) at 450 °C
3%Ru/MgO-IM	2.1	38.4	11.8	9.3	2.5
5%Ru/MgO-IM	3.5	40.7	7.0	15.8	4.7
3%Ru/MgO-DP	2.1	219.4	25.3	4.4	4.0
5%Ru/MgO-DP	3.5	168.9	33.6	3.3	3.0

Fig. 9. Arrhenius plots of the supported Ru catalysts: (■) 3%Ru/MgO-IM; (●) 5%Ru/MgO-IM; (▲) 3%Ru/MgO-DP; (▼) 5%Ru/MgO-DP.

Fig. 10. NH$_3$ conversion as a function of reaction temperature over Ru/MgO and KOH modied Ru/MgO catalysts: (■) 5%Ru/MgO-IM; (●) 5%Ru/MgO-DP; (▽) 5%Ru/MgO-DP (K/Ru = 1/1); (△) 5%Ru/MgO-DP (K/Ru = 1/2).

Similar with the other catalyst systems for NH$_3$ synthesis and NH$_3$ decomposition, the TOF values of both Ru/MgO-IM and Ru/MgO-DP catalysts show obvious increase with increase of Ru particle sizes. This favorable performance mainly arose from the appropriate crystal size of the synthesized Ru nanoparticles.

3.2.6. TEM

The influence of preparation method on the particle size and morphology of Ru nanoparticles was studied by TEM. Fig. 8 shows representative TEM images of Ru/MgO-IM and mesoporous Ru/MgO-DP samples with different Ru loadings. The Ru nanoparticles are homogenously distributed on the surface of the MgO support for Ru/MgO-IM catalysts. Compared with reduced Ru/MgO-IM samples, much uniform Ru particle size distributions can be observed for the mesoporous Ru/MgO-DP samples. The particle size distribution and average diameter of Ru particles for the different reduced Ru/MgO samples can be obtained by measuring around 200 particles taken from TEM images (Fig. S2). The average size of Ru particles of 3%Ru/MgO-DP and 5%Ru/MgO-DP catalysts are 5.6 and 3.8 nm. Increase of Ru content has no apparent effect on the particle size distribution of Ru nanoparticles, and similar particle size distributions (histograms in Fig. S2) can be observed with Ru content varies from 2.0 to 3.5 wt.%. TEM results show that average particle sizes for 3%Ru/MgO-DP and 5%Ru/MgO-DP are both smaller than those of Ru/MgO-IM samples (7.6 and 9.6 nm, respectively). Consistent with CO chemisorption results, TEM further evidences that DP method leads a much enhanced dispersion of Ru for mesoporous Ru/MgO-DP catalysts in comparison with that of the Ru/MgO-IM catalysts.

3.2.7. Kinetic test

Fig. 9 shows Arrhenius-type plots for the rates of NH$_3$ decomposition reaction over the Ru/MgO-IM and mesoporous Ru/MgO-DP catalysts. The apparent activation energies of the 3%Ru/MgO-IM and 5%Ru/MgO-IM catalysts are 119.3 and 102.7 kJ/mol; respec-
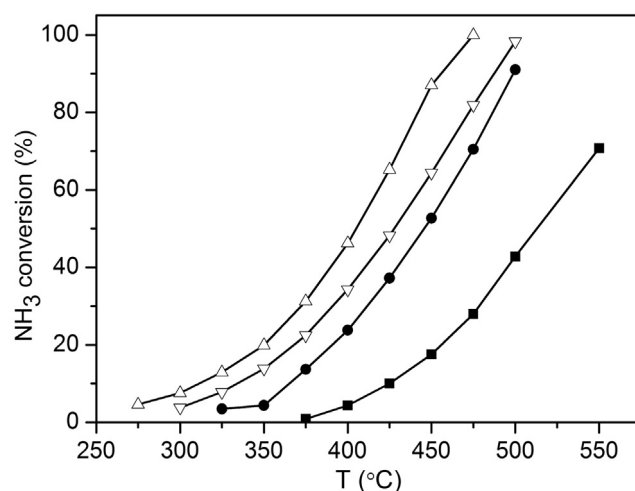
tively. The preparation method has a great influence not only on the catalytic performances of the catalysts but also on the apparent activation energies of the of mesoporous Ru/MgO catalysts. Correlating well with the catalytic activity results, a remarkable decrease of apparent activation energies can be observed for mesoporous Ru/MgO-DP catalysts. The 3%Ru/MgO-DP and 5%Ru/MgO-DP catalysts show apparent activation energies of about 105.6 and 83.3 kJ/mol, which are much smaller than those of corresponding Ru/MgO-IM samples with similar Ru content.

3.3. Effect of KOH as modifying agent for 5%Ru/MgO-DP catalyst

Due to the electron donation of alkali or alkaline earth ions, alkali or alkaline earth ions have been demonstrated as efficient promoters for supported Ru or Fe catalysts. The associative desorption of nitrogen atoms from the catalyst surface is the rate-determining step for NH$_3$ decomposition. Unlike the reverse NH$_3$ synthesis reaction, the K$^+$ ions are found to be more effective than Ba^{2+} ions for promoting Ru in NH$_3$ decomposition [23,44]. Here, KOH was applied as the promoter to modify the reduced 5%Ru/MgO(DP) catalyst. As shown in Fig. 10, KOH modification leads to a remarkable increase in the NH$_3$ conversion for 5%Ru/MgO-DP catalyst. Furthermore, the molar ratio K/Ru has an obvious influence on the catalytic activity of the 5%Ru/MgO-DP catalyst. The NH$_3$ conversion over KOH-5%Ru/MgO-DP (K/Ru = 1/2) can reach 99.9% at 475 °C, which is much higher than that of 5%Ru/MgO-DP sample (70.5%). Further addition of KOH into the reduced 5%Ru/MgO-DP catalyst led to an obvious decrease of catalytic activity for KOH-5%Ru/MgO-DP (K/Ru = 1/1) (80.9%), which may result from the decrease of catalytically active Ru sites being covered with KOH species located on the surface of metal particles, and have also been observed for the alkali modified Ru/CNT catalyst [23] (Table 3).

Modification of 5%Ru/MgO-DP with KOH can not only enhance the catalytic activity but also result in a decline in apparent acti-

Table 3

NH_3 conversion and H_2 formation rate (mmol H_2/gcat·min over 5%Ru/MgO-DP and Ru/CNTs catalysts at atmospheric pressure.

T, °C	NH_3 conversion, %				H_2 formation rate, mmol H_2/gcat·min			
	5%Ru/MgO-DP[a]	K-5%Ru/MgO-DP[a]	Ru/CNTs[b]	K-Ru/CNTs[b]	5%Ru/MgO-DP[a]	K-5%Ru/MgO-DP[a]	Ru/CNTs[b]	K-Ru/CNTs[b]
400	23.8	46.2	17.0	57.9	9.6	18.6	5.7	19.4
450	52.7	87.0	43.3	97.4	21.2	35.0	14.5	32.6
475	70.5	100	–	–	28.3	40.2	–	–
500	91.0	–	84.8	–	36.6	–	28.4	–
550	100	–	99.8	–	40.2	–	33.4	–

[a] Conditions: pure NH_3, GHSV = 36,000 mL/gcat h, catalyst loading 50 mg. The calculation of H_2 formation rate was based on the weight of the reduced 5%Ru/MgO-DP catalyst.

[b] Conditions: pure NH_3, GHSV = 30,000 mL/gcat h, catalyst loading 50 mg. Reaction data taken from literature 16.
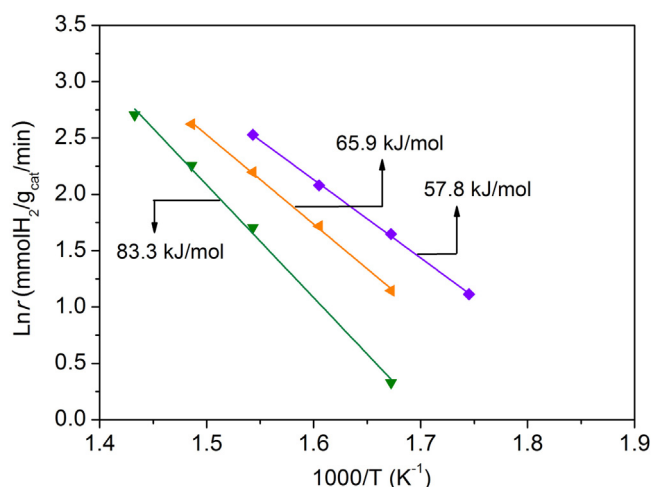

Fig. 11. Arrhenius plots of the 5%Ru/MgO-DP and KOH modified 5%Ru/MgO-DP catalysts: (▼) 5%Ru/MgO-DP; (◄) 5%Ru/MgO-DP (K/Ru = 1/1); (♦) 5%Ru/MgO-DP (K/Ru = 1/2).

vation energy value (Fig. 11) [23]. The Ea values of KOH modified 5%Ru/MgO-DP are much smaller than that of the 5%Ru/MgO-DP (83.3 kJ/mol). Among the Ru/MgO catalysts investigated here, the KOH-5%Ru/MgO-DP (K/Ru = 1/2) has a smallest Ea of 57.8 kJ/mol, which correlates well with the highest catalytic activity of the KOH-5%Ru/MgO-DP (K/Ru = 1/2). The apparent energy over KOH modified 5%Ru/MgO-DP is 57.8 kJ/mol, which are comparable with that of the alkali modifed Ru/CNTs catalysts (54 kJ/mol) [45]. Here, the much enhanced activity of the KOH modified 5%Ru/MgO-DP catalyst can be attributed to a change in the electronic property of the metallic Ru rather than the change in morphology of the Ru particles. Up to now, K-Ru/CNTs catalysts have been demonstrated to the most active catalysts in the previous literatures [45]. A comparison of Ru/MgO-DP catalyst with Ru/CNTs catalysts under similar reaction condition is listed in Table 2. The 5%Ru/MgO-DP catalyst possesses higher catalytic activity than the Ru/CNTs catalysts reported by Yin et al. [45]. Most importantly, the H_2 formation rates of 5%Ru/MgO-DP and KOH modified 5%Ru/MgO-DP catalyst is about 1.2–1.7 times higher than that of the Ru/CNTs and K modified Ru/CNTs catalyst under similar condition.

4. Conclusions

In conclusion, we have developed a deposition-precipitation method for the preparation of highly active mesoporous Ru/MgO catalysts for NH_3 decomposition reaction. The obtained mesoporous Ru/MgO catalysts have high surface area, small Ru particle size and enhanced metal-support interaction. As a result of the unique mesoporous structure and abundant exposed Ru sites, mesoporous Ru/MgO catalysts exhibit excellent catalytic performance for NH_3 decomposition reaction with a high activity and stability. Addi-

tion of KOH can effectively enhance the catalytic activity of the Ru/MgO-DP catalysts, and the optimal amount was determined to be K/Ru = 1/2. The KOH modified mesoporous Ru/MgO-DP catalyst gives comparable catalytic performance with one of the most efficient K-Ru/CNTs catalysts under similar reaction condition. This work offers a facile, low-cost and environment-friendly strategy towards production of highly efficient mesoporous Ru/MgO catalyst for producing CO_x-free hydrogen from NH_3 decomposition reaction.

Appendix A. Supplementary data

Supplementary data associated with this article can be found, in the online version, at http://dx.doi.org/10.1016/j.apcatb.2017.04.043.

References

[1] A. Klerke, C.H. Christensen, J.K. Norskov, T. Vegge, Ammonia for hydrogen storage: challenges and opportunities, J. Mater. Chem. 18 (2008) 2304–2310.

[2] R. Lan, J.T.S. Irvine, S.W. Tao, Ammonia and related chemicals as potential indirect hydrogen storage materials, Int. J. Hydrogen Energy 37 (2012) 1482–1494.

[3] R. Metkemeijer, P. Achard, Comparison of ammonia and methanol applied indirectly in a hydrogen fuel-cell, Int. J. Hydrogen Energy 19 (1994) 535–542.

[4] R. Metkemeijer, P. Achard, Ammonia as a feedstock for a hydrogen fuel-cell – reformer and fuel-cell behavior, J. Power Sources 49 (1994) 271–282.

[5] B.L. Yi, Fuel Cell—Principle, Technology and Application, Chemical Industry Press, Beijing, 2003, pp. 2.

[6] R.O. Idem, N.N. Bakhshi, Production of hydrogen from methanol. 1. Catalyst characterization studies, Ind. Eng. Chem. Res. 33 (1994) 2047–2055.

[7] A.S. Chellappa, C.M. Fischer, W.J. Thomson, Ammonia decomposition kinetics over Ni-Pt/Al2O3 for PEM fuel cell applications, Appl. Catal. A: Gen. 227 (2002) 231–240.

[8] T.V. Choudhary, D.W. Goodman, Stepwise methane steam reforming: a route to CO-free hydrogen, Catal. Lett. 59 (1999) 93–94.

[9] V.R. Choudhary, B.S. Uphade, A.S. Mamman, Oxidative conversion of methane to syngas over nickel supported on commercial low surface area porous catalyst carriers precoated with alkaline and rare earth oxides, J. Catal. 172 (1997) 281–293.

[10] J.N. Armor, The multiple roles for catalysis in the production of H-2, Appl. Catal. A: Gen. 176 (1999) 159–176.

[11] T.V. Choudhary, C. Sivadinarayana, D.W. Goodman, Catalytic ammonia decomposition: COx-free hydrogen production for fuel cell applications, Catal. Lett. 72 (2001) 197–201.

[12] M.E.E. Abashar, Y.S. Al-Sughair, I.S. Al-Mutaz, Investigation of low temperature decomposition of ammonia using spatially patterned catalytic membrane reactors, Appl. Catal. A: Gen. 236 (2002) 35–53.

[13] S.F. Yin, B.Q. Xu, C.F. Ng, C.T. Au, Nano Ru/CNTs: a highly active and stable catalyst for the generation of COx-free hydrogen in ammonia decomposition, Appl. Catal. B–Environ. 48 (2004) 237–241.

[14] S.F. Yin, B.Q. Xu, X.P. Zhou, C.T. Au, A mini-review on ammonia decomposition catalysts for on-site generation of hydrogen for fuel cell applications, Appl. Catal. A: Gen. 277 (2004) 1–9.

[15] S.F. Yin, Q.H. Zhang, B.Q. Xu, W.X. Zhu, C.F. Ng, C.T. Au, Investigation on the catalysis of COx-free hydrogen generation from ammonia, J. Catal. 224 (2004) 384–396.
[16] S.F. Yin, B.Q. Xu, S.J. Wang, C.F. Ng, C.T. Au, Magnesia-carbon nanotubes (MgO-CNTs) nanocomposite: novel support of Ru catalyst for the generation of COx-free hydrogen from ammonia, Catal. Lett. 96 (2004) 113–116.
[17] J.G. Choi, J. Ha, J.W. Hong, Synthesis and catalytic properties of vanadium interstitial compounds, Appl. Catal. A: Gen. 168 (1998) 47–56.
[18] C.H. Liang, W.Z. Li, Z.B. Wei, Q. Xin, C. Li, Catalytic decomposition of ammonia over nitrided MoNx/alpha-Al2O3 and NiMoNy/alpha-Al2O3 catalysts, Ind. Eng. Chem. Res. 39 (2000) 3694–3697.
[19] J.G. Choi, M.K. Jung, S. Choi, T.K. Park, I.H. Kuk, J.H. Yoo, H.S. Park, H.S. Lee, D.H. Ahn, H.S. Chung, Synthesis and catalytic properties of vanadium nitrides, Bull. Chem. Soc. Jpn. 70 (1997) 993–996.
[20] J.P. Guo, P.K. Wang, G.T. Wu, A.A. Wu, D.Q. Hu, Z.T. Xiong, J.H. Wang, P. Yu, F. Chang, Z. Chen, P. Chen, Lithium imide synergy with 3d transition-metal nitrides leading to unprecedented catalytic activities for ammonia decomposition, Angew. Chem. Int. Ed. 54 (2015) 2950–2954.
[21] J.P. Guo, F. Chang, P.K. Wang, D.Q. Hu, P. Yu, G.T. Wu, Z.T. Xiong, P. Chen, Highly active mnN-Li2NH composite catalyst for producing COx-free hydrogen, ACS Catal. 5 (2015) 2708–2713.
[22] B. Lorenzut, T. Montini, M. Bevilacqua, P. Fornasiero, FeMo-based catalysts for H-2 production by NH3 decomposition, Appl. Catal. B–Environ. 125 (2012) 409–417.
[23] S.J. Wang, S.F. Yin, L. Li, B.Q. Xu, C.F. Ng, C.T. Au, Investigation on modification of Ru/CNTs catalyst for the generation of COx-free hydrogen from ammonia, Appl. Catal. B–Environ. 52 (2004) 287–299.
[24] J.C. Ganley, F.S. Thomas, E.G. Seebauer, R.I. Masel, A priori catalytic activity correlations: the difficult case of hydrogen production from ammonia, Catal. Lett. 96 (2004) 117–122.
[25] A.K. Hill, L. Torrente-Murciano, Low temperature H-2 production from ammonia using ruthenium-based catalysts: synergetic effect of promoter and support, Appl. Catal. B–Environ. 172 (2015) 129–135.
[26] X.Z. Duan, G. Qian, X.G. Zhou, Z.J. Sui, D. Chen, W.K. Yuan, Tuning the size and shape of Fe nanoparticles on carbon nanofibers for catalytic ammonia decomposition, Appl. Catal. B–Environ. 101 (2011) 189–196.
[27] D. Varisli, N.G. Kaykac, COx free hydrogen production over cobalt incorporated silicate structured mesoporous catalysts, Appl. Catal. B–Environ. 127 (2012) 389–398.
[28] W.Q. Zheng, J. Zhang, Q.J. Ge, H.Y. Xu, W.Z. Li, Effects of CeO2 addition on Ni/Al2O3 catalysts for the reaction of ammonia decomposition to hydrogen, Appl. Catal. B–Environ. 80 (2008) 98–105.
[29] Q. Su, L.L. Gu, Y. Yao, J. Zhao, W.J. Ji, W.P. Ding, C.T. Au, Layered double hydroxides derived Ni-x(MgyAlzOn) catalysts: enhanced ammonia decomposition by hydrogen spillover effect, Appl. Catal. B–Environ. 201 (2017) 451–460.
[30] F. Hayashi, Y. Toda, Y. Kanie, M. Kitano, Y. Inoue, T. Yokoyama, M. Hara, H. Hosono, Ammonia decomposition by ruthenium nanoparticles loaded on inorganic electride C12A7:e(−), Chem. Sci. 4 (2013) 3124–3130.
[31] Y.X. Li, L.H. Yao, Y.Y. Song, S.Q. Liu, J. Zhao, W.J. Ji, C.T. Au, Core-shell structured microcapsular-like Ru@SiO2 reactor for efficient generation of COx-free hydrogen through ammonia decomposition, Chem. Commun. 46 (2010) 5298–5300.
[32] X.K. Li, W.J. Ji, J. Zhao, S.J. Wang, C.T. Au, Ammonia decomposition over Ru and Ni catalysts supported on fumed SiO$_2$, MCM-41, and SBA-15, J. Catal. 236 (2005) 181–189.
[33] G. Li, M. Kanezashi, T. Tsuru, Highly enhanced ammonia decomposition in a bimodal catalytic membrane reactor for COx-free hydrogen production, Catal. Commun. 15 (2011) 60–63.
[34] J. Okal, M. Zawadzki, L. Kepinski, L. Krajczyk, W. Tylus, The use of hydrogen chemisorption for the determination of Ru dispersion in Ru/gamma-alumina catalysts, Appl. Catal. A: Gen. 319 (2007) 202–209.
[35] Y.V. Larichev, Effect of Cs+ promoter in Ru/MgO catalysts, J. Phys. Chem. C 115 (2011) 631–635.
[36] L. Li, Z.H. Zhu, Z.F. Yan, G.Q. Lu, L. Rintoul, Catalytic ammonia decomposition over Ru/carbon catalysts: the importance of the structure of carbon support, Appl. Catal. A: Gen. 320 (2007) 166–172.
[37] F.R. Garcia-Garcia, J. Alvarez-Rodriguez, I. Rodriguez-Ramos, A. Guerrero-Ruiz, The use of carbon nanotubes with and without nitrogen doping as support for ruthenium catalysts in the ammonia decomposition reaction, Carbon 48 (2010) 267–276.
[38] J. Zhang, H.Y. Xu, Q.J. Ge, W.Z. Li, Highly efficient Ru/MgO catalysts for NH3 decomposition: synthesis, characterization and promoter effect, Catal. Commun. 7 (2006) 148–152.
[39] S. Zhang, X.S. Li, B.B. Chen, X.B. Zhu, C. Shi, A.M. Zhu, CO oxidation activity at room temperature over Au/CeO2 catalysts: disclosure of induction period and humidity effect, ACS Catal. 4 (2014) 3481–3489.
[40] M.L. Toebes, F.F. Prinsloo, J.H. Bitter, A.J. van Dillen, K.P. de Jong, Influence of oxygen-containing surface groups on the activity and selectivity of carbon nanofiber-supported ruthenium catalysts in the hydrogenation of cinnamaldehyde, J. Catal. 214 (2003) 78–87.
[41] S. Murata, K. Aika, Preparation and characterization of chlorine-free ruthenium catalysts and the promoter effect in ammonia-synthesis. 1. An alumina-supported ruthenium catalyst, J. Catal. 136 (1992) 110–117.
[42] C.H. Liang, Z.B. Wei, Q. Xin, C. Li, Ammonia synthesis over Ru/C catalysts with different carbon supports promoted by barium and potassium compounds, Appl. Catal. A: Gen. 208 (2001) 193–201.
[43] A.M. Karim, V. Prasad, G. Mpourmpakis, W.W. Lonergan, A.I. Frenkel, J.G.G. Chen, D.G. Vlachos, Correlating particle size and shape of supported Ru/gamma-Al2O3 catalysts with NH3 decomposition activity, J. Am. Chem. Soc. 131 (2009) 12230–12239.
[44] Z. Kowalczyk, S. Jodzis, W. Rarog, J. Zielinski, J. Pielaszek, Effect of potassium and barium on the stability of a carbon-supported ruthenium catalyst for the synthesis of ammonia, Appl. Catal. A: Gen. 173 (1998) 153–160.
[45] S.F. Yin, B.Q. Xu, W.X. Zhu, C.F. Ng, X.P. Zhou, C.T. Au, Carbon nanotubes-supported Ru catalyst for the generation of COx-free hydrogen from ammonia, Catal. Today 93–95 (2004) 27–38.